

Is shrub expansion into grasslands pushed or pulled? A
spatial integral projection model for woody plant
encroachment

Trevor Drees^{*a,b}, Brad M. Ochocki^b, Scott L. Collins^c, and Tom E.X. Miller^b

^aDepartment of Biology, Penn State University, State College, PA USA

^bProgram in Ecology and Evolutionary Biology, Department of BioSciences, Rice
University, Houston, TX USA

^cDepartment of Biology, University of New Mexico, Albuquerque, NM USA

May 1, 2022

^{*}thd5066@psu.edu

1 Abstract

2 **Encroachment**¹ of shrubs into adjacent grasslands has become an increasingly reported
3 phenomenon across the world, and such encroachment is either pulled forward by high
4 population growth at the low-density encroachment front or pushed forward by higher-
5 density areas behind the front. However, at sites such as Sevilleta National Wildlife
6 Refuge in central New Mexico, little is known about whether encroachment is pushed or
7 pulled, and the dynamics of encroachment are not well-understood. Here, long-term en-
8 croachment of creosotebush (*Larrea tridentata*), a native perennial shrub, stands in stark
9 contrast with the stagnation in encroachment observed in recent decades. In order to
10 better understand creosotebush encroachment at this site, we quantify it using a spatially
11 structured population model where a wave of individuals travels at a speed governed by
12 both dispersal and density-dependence. Results indicate that population growth rates
13 generally increase with decreasing density, suggesting that encroachment is pulled by
14 individuals at the low-density wave front, and the spatial population model predicts an
15 encroachment rate of less than 2 cm per year. While the predicted rate of encroach-
16 ment is consistent with observations over recent decades, it does not explain long-term
17 creosotebush encroachment at the study site, suggesting that this process may occur in
18 pulses when recruitment, seedling survival, or dispersal significantly exceed typical rates.
19 Overall, our work demonstrates that individuals at low densities are likely the biggest
20 contributors to creosotebush encroachment at this site, and that this encroachment is
21 likely a process that occurs in large but infrequent bursts rather than at a steady pace.

22 Keywords

23 density-dependence, ecotones, woody encroachment, shrubs, integral projection model,
24 grassland

¹*I am not editing the abstract for now.*

25 Introduction

26 The recent and ongoing encroachment of shrubs and other woody plants into adjacent
27 grasslands has caused significant vegetation changes across arid and semi-arid landscapes
28 worldwide (Van Auken, 2000, 2009; Goslee et al., 2003; Gibbens et al., 2005; Parizek et al.,
29 2002; Cabral et al., 2003; Trollope et al., 1989; Roques et al., 2001). The process of en-
30 croachment generally involves increases in the number or density of woody plants in both
31 time and space (Van Auken, 2000), which can drive shifts in plant community structure
32 and alter ecosystem processes (Schlesinger et al., 1990; Ravi et al., 2009; Schlesinger
33 and Pilmanis, 1998; Knapp et al., 2008). Other effects of encroachment include changes
34 in ecosystem services (Reed et al., 2015; Kelleway et al., 2017), declines in biodiversity
35 (Ratajczak et al., 2012; Sirami and Monadjem, 2012; Brandt et al., 2013), and economic
36 losses in areas where the proliferation of shrubs adversely affects grazing land and pastoral
37 production (Mugasi et al., 2000; Oba et al., 2000).

38 Woody plant encroachment can be studied through the lens of spatial population
39 biology as a wave of individuals that may expand across space and over time (Kot et al.,
40 1996; Neubert and Caswell, 2000; Wang et al., 2002; Pan and Lin, 2012). Theory pre-
41 dicts that the speed of wave expansion depends on two processes: local demography and
42 dispersal of propagules. First, local demographic processes include recruitment, survival,
43 growth, and reproduction, which collectively determine the rate at which newly colonized
44 locations increase in density and produce new propagules. Second, colonization events
45 are driven by the spatial dispersal of propagules, which is commonly summarized as a
46 probability distribution of dispersal distance, or “dispersal kernel”. The speed at which
47 expansion waves move is highly dependent upon the shape of the dispersal kernel, espe-
48 cially long-distance dispersal events in the tail of the distribution (Skarpaas and Shea,
49 2007). Both demography and dispersal may depend on plant size, since larger plants
50 often have improved demographic performance and release seeds from greater heights,

51 leading to longer dispersal distances (Nathan et al., 2011). Accounting for population
52 structure, including size structure, may therefore be important for understanding and
53 predicting wave expansion dynamics (Neubert and Caswell, 2000).

54 Theory predicts that the nature of conspecific density dependence is another critical
55 feature of expansion dynamics but this is rarely studied in the context of woody plant
56 encroachment. Expansion waves typically correspond to gradients of conspecific density
57 – high in the back and low at the front – and demographic rates may be sensitive to
58 density due to intraspecific interactions like competition or facilitation. If the demo-
59 graphic effects of density are strictly negative due to competitive effects that increase
60 with density then demographic performance is maximized as density goes to zero, at the
61 leading edge of the wave. Under these conditions, the wave is “pulled” forward by indi-
62 viduals at the low-density vanguard (Kot et al., 1996), and targeting these individuals
63 and locations would be the most effective way to slow down or prevent encroachment
64 (cite?). However, woody encroachment systems often involve positive feedbacks whereby
65 shrub establishment modifies the environment in ways that facilitate further shrub re-
66 cruitment. For example, woody plants can modify their micro-climates in ways that
67 elevate nighttime minimum temperatures, promoting conspecific recruitment and sur-
68 vival for freeze-sensitive species (D’Odorico et al., 2010; Huang et al., 2020). Positive
69 density dependence (or Allee effects) causes demographic rates to be maximized at higher
70 densities behind the leading edge, which “push” the expansion forward, leading to qualita-
71 tively different expansion dynamics (Kot et al., 1996; Taylor and Hastings, 2005; Sullivan
72 et al., 2017; Lewis and Kareiva, 1993; Veit and Lewis, 1996; Keitt et al., 2001). Pushed
73 expansion waves generally have different shapes (steeper density gradients) and slower
74 speeds than pulled waves (Gandhi et al., 2016), and may require different strategies for
75 managing or decelerating expansion (check Taylor and Hastings ref). The potential for
76 positive feedbacks is well documented in woody encroachment systems but it remains un-
77 clear whether and how strongly these feedbacks decelerate shrub expansion and influence

78 strategies for management of woody encroachment.

79 In this study, we linked woody plant encroachment to ecological theory for invasion
80 waves, with the goals of understanding how seed dispersal and density-dependent demog-
81 raphy drive encroachment, and determining whether the encroachment wave is pushed or
82 pulled. Throughout the aridlands of the southwestern United States, shrub encroachment
83 into grasslands is well documented (cite) but little is known about the dispersal and de-
84 mographic processes that govern it. Our work focused on encroachment of creosotebush
85 (*Larrea tridentata*) in the northern Chihuahuan Desert. Expansion of this species into
86 grasslands over the past 150 years has been well documented, leading to decreased cover
87 of *Bouteloua eriopoda*, the dominant foundation species of Chihuahuan desert grassland
88 (Gardner, 1951; Buffington and Herbel, 1965; Gibbens et al., 2005). As in many woody
89 encroachment systems, creosotebush expansion generates ecotones marking a transition
90 from dense shrubland to open grassland, with a transition zone in between where shrubs
91 can often be found interspersed among grasses (Fig. 1).

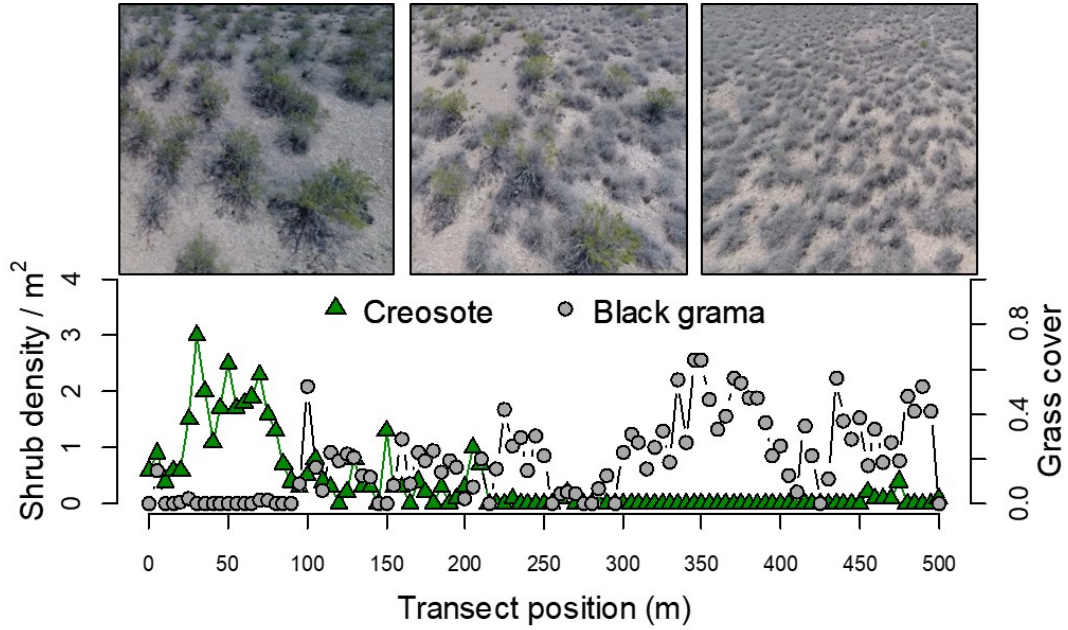


Figure 1: Example of an ecotone transect at Sevilleta LTER, spanning gradients of creosotebush and black grama grass.

Historically, creosotebush encroachment into grasslands is believed to have been driven by a combination of factors including overgrazing, drought, variability in rainfall, and suppression of fire regimes Moreno-de las Heras et al. (2016). These shrubs are also thought to further facilitate their own encroachment through positive feedbacks (Grover and Musick, 1990; D’Odorico et al., 2012) by modifying their environment in ways that favor continued growth and recruitment, including changes to the local micro-climate (D’Odorico et al., 2010) and rates of soil erosion (Turnbull et al., 2010). Such positive feedback also involve suppression of herbaceous competitors, reducing competition as well as the amount of flammable biomass used to fuel the fires that keep creosotebush growth in check (Van Auken, 2000). We hypothesized that, given potential for positive feedback mechanisms, the rarity of conspecifics at the low-density encroachment front may depress demographic performance and generate pushed-wave dynamics.

104 We used a combination of observational and experimental data from shrub ecotones
 105 in central New Mexico to parameterize a spatial integral projection model (SIPM) that
 106 predicts that speed of encroachment (m/yr) resulting from lower-level demographic and
 107 dispersal processes. Our data came from demographic surveys and experimental trans-
 108 plants along replicate ecotone transects spanning a gradient of shrub density, and seed
 109 drop experiments to infer the properties of the dispersal kernel. We focused on wind
 110 dispersal of seeds as a starting point, since little is known about the natural history
 111 of dispersal in this system and the seeds lack rewards to attract animal dispersers. We
 112 also used re-surveys of permanent transects as an independent measure of encroachment
 113 that provided a benchmark against which to evaluate model predictions. The SIPM ac-
 114 counts for size-structured demography of creosotebush, allows us to test whether shrub
 115 expansion is pulled by the low-density front or pushed from the high-density core, and
 116 identifies the local (demographic) and spatial (seed dispersal) life cycle transitions that
 117 most strongly contribute to expansion speed². We address the following specific ques-
 118 tions:

- 119 1. What is the nature of conspecific density dependence in demographic vital rates
 120 along shrub encroachment ecotones? Is encroachment pulled by the individuals at
 121 the front of the wave or pushed by individuals behind it?
- 122 2. What is the wind dispersal kernel for this species and how far do seeds typically
 123 travel by wind?
- 124 3. What is the predicted rate of expansion from the SIPM and what lower-level pro-
 125 cesses most strongly govern the expansion speed?
- 126 4. How does the observed rate of encroachment in recent past compare to model
 127 predictions?

²*we will need to stay consistent with the language of encroachment/expansion/invasion. For now I am switching a lot.*

128 **Materials and methods**

129 **Study species**

130 Creosotebush *Larrea tridentata* is a perennial, drought-resistant shrub that is native to
131 the arid and semiarid regions of the southwestern United States and northern Mexico.
132 High-density areas of creosotebush consist largely of barren soil between plants due to
133 the “islands of fertility” these shrubs create around themselves (Schlesinger et al., 1996;
134 Reynolds et al., 1999), though lower-density areas will often contain grasses in the inter-
135 shrub spaces (Fig. 1). In our northern Chihuahuan desert study region creosotebush
136 reproduces sexually, with numerous small yellow flowers giving rise to highly pubescent
137 spherical fruits several millimetres in diameter; these fruits consist of five carpels, each
138 of which contains a single seed. Seeds are dispersed from the parent plant by gravity
139 and wind, with the possibility for seeds to also be blown across the soil surface or trans-
140 ported by water runoff (Maddox and Carlquist, 1985). In other regions, this species also
141 reproduces asexually and can give rise to long-lived clonal stands (Vasek, 1980), but this
142 does not occur in our study region. The foliage is dark green, resinous, and unpalatable
143 to most grazing and browsing animals (Mabry et al., 1978).

144 **Study site**

145 We conducted our experiments and censuses at the Sevilleta National Wildlife Refuge
146 (SNWR), a Long-Term Ecological Research (LTER) site in central New Mexico. The
147 refuge exists at the intersection of several eco-regions, including the Chihuahuan Desert
148 and steppes of the Colorado Plateau. Annual precipitation is low at approximately
149 250 mm, with the majority falling during the summer monsoon season from June to
150 September.

151 Significant creosotebush encroachment at SNWR last occurred in the 1950’s, with
152 high shrub recruitment before and after a multi-year drought that caused a large loss

153 in grass cover, likely setting the stage for creosotebush expansion (Moreno-de Las Heras
154 et al., 2015; Moreno-de las Heras et al., 2016). The recruitment events that facilitate cre-
155 osotebush expansion are thought to be highly episodic (Peters and Yao, 2012). Given that
156 creosotebush seedlings have been shown to establish around the time that late-summer
157 heavy rainfall occurs (Boyd and Brum, 1983; Bowers et al., 2004), higher precipitation
158 rates may be responsible for increased recruitment.

159 **Encroachment re-surveys**

160 We recorded shrub percent cover along two permanent 1000-m transects that spanned
161 the shrub-grass ecotone, from high to low to near-zero shrub density. These surveys were
162 conducted in summer 2001 and again in summer 2013 to document change in creosotebush
163 abundance and spatial extent. At every 10 meters, shrub cover was recorded in nine cover
164 classes ($<1\%$, $1-4\%$, $5-10\%$, $10-25\%$, $25-33\%$, $33-50\%$, $50-75\%$, $75-95\%$, $>95\%$). For
165 visualization, we show midpoint values of these cover classes at each meter location for
166 both transects and years.

167 **Demographic data**

168 **Ecotone transects**

169 Collection of demographic data occurred during early June of every year from 2013-2017.
170 This work was conducted at four sites in the eastern part of SNWR (one site was initiated
171 in 2013 and the other three in 2014), with three transects at each site (different transects
172 than those used for re-surveys). All transects were placed along a shrubland-grassland
173 ecotone so that a full range of shrub densities was captured: each transect spanned
174 core shrub areas, grassland with few shrubs, and the transition between them. Lengths
175 of these transects varied from 200 to 600 m, determined by the strength of vegetation
176 transition since “steep” transitions required less length to capture the full range of shrub
177 densities.

178 We quantified shrub density in 5-meter “windows” along each transect, including all
179 shrubs within one meter of the transect on either side. Densities were quantified once for
180 each transect (in 2013 or 2014) and were assumed to remain constant for the duration
181 of the study, a reasonable assumption for a species with very low recruitment and very
182 high survival of established plants. Given the population’s size structure, we weighted
183 the density of each window by the sizes of the plants, which we quantified as volume
184 (cm^3). Volume was calculated as that of an elliptic cone: $V_i = \frac{\pi h}{3} \frac{lw}{4}$ where l , w , and h
185 are the maximum length, maximum width, and height, respectively. Maximum length
186 and width were measured so that they were always perpendicular to each other, and
187 height was measured from the base of the woody stem at the soil surface to the highest
188 part of the shrub. The weighted density for a window was then expressed as $\log(\text{volume})$
189 summed over all plants in the window.

190 **Observational census**

191 At 50-m intervals along each transect we tagged up to 10 plants for annual demographic
192 census and recorded their local (5-m resolution) window so that we could connect indi-
193 vidual demographic performance to local weighted density. These tagged shrubs were
194 revisited every June and censused for survival (alive/dead), size (width, length, and
195 height, as above), and reproduction (numbers of flowers and fruits). In instances where
196 shrubs had large numbers of reproductive structures that would be difficult to reliably
197 count (a large shrub may have thousands of flowers or fruits), we made counts on a frac-
198 tion of the shrub and extrapolated to estimate whole-plant reproduction. Creosotebush
199 does not have a discrete reproductive season, instead producing flowers and fruits over
200 much of the warm season. Our measurements of reproductive output are therefore con-
201 servative, and likely underestimate cumulative seed production for an entire transition
202 year. Each year, we searched for new recruits within one m on either side of the transect.
203 New recruits were tagged and added to the demographic census.

204 Transplant experiment

205 We conducted a transplant experiment in 2015 to test how shrub density affects seedling
206 survival. This approach complemented observational estimates of density dependence
207 and filled in gaps for a part of the shrub life cycle that is rarely observed due to low re-
208 cruitment. Seeds for the experiment were collected from plants in our study population in
209 2014. Seeds were germinated on Pro-Mix potting soil (Quakertown, PA) in Fall 2014 and
210 seedlings were transferred to 3.8 cm-by-12.7 cm cylindrical containers and maintained in
211 a greenhouse at Rice University. Seedlings were transported to SNWR and transplanted
212 into our experimental design during July 27-31, 2015. Transplant timing was intended
213 to coincide with the start of the monsoon season, when most natural recruitment occurs.

214 The transplant experiment was conducted at the same four sites and three transects
215 per site as the observational demographic census, where we knew weight shrub densities
216 at 5-m window resolution. Along each transect we established 12 1-m by 1-m plots.
217 Plots were intentionally placed to capture density variation: four plots were in windows
218 with zero shrubs, four plots were placed in the top four highest-density windows on the
219 transect, and the remaining four plots were randomly distributed among the remaining
220 windows with weighted density greater than zero. Plots were placed in the middle of
221 each 5-m window (at meter 2.5) and were divided into four 0.5-m by 0.5-m subplots. We
222 divided each subplot into nine squares and recorded ground cover of each square as one
223 of the following categories: bare, creosotebush, black grama (*B. eriopoda*), blue grama
224 (*B. gracilis*), other grass, or “other”. Each subplot received one transplanted subplot, for
225 a total of 48 transplants per transect, 144 transplants per site, and 576 transplants in
226 the entire experiment. Each site was set up on a different day and there was a significant
227 monsoon event after the third and before the fourth site. This resulted in differential
228 mortality that appears to be related to site (the soil was moist at the fourth site at the
229 time of transplanting, which favored survival) but more likely reflects the timing of the
230 monsoon event relative to planting. We revisited the transplant experiment on October

231 24, 2015 to survey mortality. After that first visit, transplants were censused along with
232 the naturally occurring plants each June, following the methods described above.

233 **Demographic analysis**

234 We fit statistical models to the demographic data and used AIC-based model selection to
235 evaluate empirical support for alternative candidate models. The top statistical models
236 were then used as the vital rate sub-models of the SIPM, so there is a strong connection
237 between the statistical and population modeling, as is typical of integral projection mod-
238 eling. Our analyses focused on the following demographic vital rates: survival, growth,
239 probability of flowering, flower and fruit production, and seedling recruitment. All of
240 these except recruitment were modeled as a function of plant size, and all of them in-
241 cluded the possibility of density dependence, since we could connect the demographic
242 performance of individual shrubs to the weighted density of their transect window.

243 The alternative hypotheses of pushed versus pulled wave expansion rest on how demo-
244 graphic vital rates, and the rate of population increase (λ) derived from the combination
245 of all vital rates, respond to density. We were particularly interested in whether demo-
246 graphic performance was maximized as local density goes to zero (pulled) or at non-zero
247 densities behind the wave front (pushed). To flexibly model density dependence and
248 detect non-monotonic responses, we used generalized additive models in the R package
249 ‘mgcv’ (Wood, 2017). For each vital rate, we fit candidate models with or without a
250 smooth term for local weighted density (among other possible covariates). To avoid
251 over-fitting, we set the ‘gamma’ argument of `gam()` to 1.8, which increases the com-
252 plexity penalty, results in smoother fits (Wood, 2017), and makes our approach more
253 conservative (other gamma values yielded qualitatively similar results). We pooled data
254 across transition years for analysis. All models included the random effect of transect (12
255 transects across 4 sites); we did not attempt to model both site and transect-within-site
256 random effects due to the low numbers of each. All vital rate functions used the natural

257 logarithm of volume (cm^3) as the size variable and the sum $\log(\text{volume})$ as the weighted
258 density of a transect window.

259 **Survival** We modeled survival or mortality in year $t + 1$ as a Bernoulli random variable
260 with three candidate models for survival probability. These included smooth terms for
261 initial size in year t only (1), initial size and weighted density (3), and both smooth terms
262 plus an interaction between initial size and weighted density. We analyzed survival of
263 experimental transplants and observational census plants together in the same analyses,
264 with a fixed effect of ‘transplant’ included in all candidate models. Since recruits and thus
265 mortality events were both very rare in the observational survey, this approach allowed
266 us to “borrow strength” over both data sets to generate a predictive function for size- and
267 possibly density-dependent survival while statistically accounting for differences between
268 experimental and naturally occurring plants. Because we had additional, finer-grained
269 cover data for the transplant experiment that we did not have for the observational cen-
270 sus, we conducted an additional stand-alone analysis of transplant survival that explored
271 the influence of covariates at multiple spatial scales (Appendix).

272 **Growth** We initially modeled size in year $t + 1$ as a Gaussian random variable. There
273 were nine candidate models for growth (Table). The simplest model (1) defined the mean
274 of size in year $t + 1$ as a smooth function of size in year t and constant variance. Models
275 (2) and (3) had constant variance but the mean included smooth terms for initial size
276 and weighted density (2) or both smooth terms plus an interaction between initial size
277 and weighted density (3). Models 4-6 had the same mean structure as 1-3 but defined
278 the standard deviation of size in year $t + 1$ as a smooth function of initial size. Models
279 7-9 mirrored 4-6 and additionally included a smooth term for weighted density in the
280 standard deviation.

281 Inspection of the best-fitting growth model suggested that the data did not conform
282 well to a Gaussian distribution: there was excess kurtosis (fatter tails) relative to Gaus-

283 sian and left skew in the distribution of size in year $t + 1$ especially at small initial sizes.
 284 Therefore, we re-fit the growth model with a skewed generalized t (sgt) distribution, a
 285 five-parameter distribution on the real line that accommodates excess kurtosis and skew
 286 (R package ‘sgt’: (Davis, 2015)). We specified μ and σ of the sgt using the basis func-
 287 tions generated by the best-fit gam, and additionally modeled the λ parameter (which
 288 controls skewness) as a function of size in year t and the p and q parameters (which
 289 control kurtosis) as constants. We verified that the sgt model described the data well by
 290 simulating data from it and comparing simulated and real data (Appendix Fig).

291 **Flowering and fruit production** We modeled shrub reproductive status (vegetative
 292 or flowering) in year t as a Bernoulli random variable with three candidate models for
 293 flowering probability. These included smooth terms for current size (in year t) only (1),
 294 size and weighted density (3), and both smooth terms plus an interaction between size
 295 and weighted density. We modeled the reproductive output of flowering plants (the sum
 296 of flowerbuds, open flowers, and fruits – assuming that all of these equally contribute to
 297 overall seed production) in year t as a negative binomial random variable. There were
 298 three candidate models for mean reproductive output that corresponded to the same
 299 three candidates for flowering probability.

300 **Recruitment** We modeled seedling recruitment in each transect window as a binomial
 301 random variable given the number of total seeds produced in that window in the preced-
 302 ing year. There were two candidate models, with and without an influence of weighted
 303 density on the per-seed recruitment probability. To estimate window-level seed produc-
 304 tion, we used the best-fit models for flowering and fruit production and applied this to
 305 all plants in each window that we observed in our initial density surveys.

306 We modeled recruit size as a Gaussian-distributed random variable and fit four can-
 307 didate models including an influence of weighted density on mean, variance, both, and
 308 neither. Because we observed only 32 recruits, we were not confident in our ability to

model skewness and kurtosis of the recruit size distribution and therefore assumed a Gaussian distribution.

Density-dependent IPM

The size- and density-dependent statistical models comprised the sub-models of a density dependent Integral Projection Model (IPM) that we used to evaluate how the shrub population growth rate responded to con-specific density; we present this non-spatial model before layering on the spatial dynamics driven by seed dispersal. A basic density-independent IPM predicts the number of individuals of size x' at time $t + 1$ ($n(x', t + 1)$) based on a projection kernel (K) that gives the rates of transition from sizes x to x' from times t to $t + 1$ and is integrated over the size distribution from the minimum (L) to maximum (U) sizes. In a density-dependent IPM, components of the projection kernel may respond to population abundance and structure:

$$n(x', t + 1) = \int_L^U K(x', x, \tilde{n}(t)) n(x, t) dx \quad (1)$$

Here, $\tilde{n}(t)$ is some function of population structure $n(x, t)$ such as the total density of conspecifics ($\tilde{n}(t) = \int n(x, t) dx$) or, as in our case, total density weighted by size ($\tilde{n}(t) = \int x n(x, t) dx$). For simplicity, in the analyses that follow we do not model density as a dynamic state variable; instead, we treat density as a static covariate ($\tilde{n}(t) = \tilde{n}$) and evaluate the IPM at a range of density values. As in our statistical modeling, the size variable of the IPM (x, x') was $\log(\text{cm}^3)$.

For our model, the size- and density-dependent demographic transitions captured by the projection kernel include growth or shrinkage (g) from size x to x' conditioned on survival (s) at size x (combined growth-survival function $G(x', x, \tilde{n}) = g(x', x, \tilde{n})s(x, \tilde{n})$), and the production of new size- x' individuals from size- x parents ($Q(x', x, \tilde{n})$). Reproduction reflects the probability of flowering at size x (p), the number of seeds produced

by flowering plants (d), the per-seed probability of recruitment (r), and the size distribution of recruits (c). Collectively, the rate at which x -sized individuals produce x' -sized individuals at density \tilde{n} is given by the combined reproduction-recruitment function $Q(x', x, \tilde{n}) = p(x, \tilde{n})d(x, \tilde{n})r(\tilde{n})c(x', \tilde{n})$. Thus, we can express the projection kernel as:

$$K(x', x, \tilde{n}) = G(x', x, \tilde{n}) + Q(x', x, \tilde{n}) \quad (2)$$

For analysis, we evaluated the IPM kernel over a range of local densities from the minimum to the maximum of weighted density values from the 5-meter windows ($0 \leq \tilde{n} \leq \tilde{n}_{max}$). At each density level, we discretized the IPM kernel into a 200×200 approximating matrix and calculated the asymptotic growth rate $\lambda(\tilde{n})$ as its leading eigenvalue. We extended the lower (L) and upper (U) integration limits to avoid unintentional “eviction” using the floor-and-ceiling method (Williams et al., 2012).

We sought to characterize the shape of density dependence: whether fitness declined monotonically or not with increasing density. We quantified uncertainty in the density-dependent growth rate $\lambda(\tilde{n})$ by bootstrapping our data. For each bootstrap, we randomly sampled 75% of our demographic data, re-ran the statistical modeling and model selection, and used the top vital rate models to generate $\lambda(\tilde{n})$ for that data subset. We repeated this procedure for 500 bootstrap replicates.

Dispersal modelling

WALD dispersal model Dispersal kernels were calculated using the WALD, or Wald analytical long-distance dispersal, model that uses a mechanistic approach to predict dispersal patterns of plant propagules by wind. The WALD model, which is based in fluid dynamics, can serve as a good approximation of empirically-determined dispersal kernels (Katul et al., 2005; Skarpaas and Shea, 2007) and may be used when direct observations of dispersal are not available. Under the assumptions that wind turbulence is low, wind

flow is vertically homogenous, and terminal velocity is achieved immediately upon seed release, the WALD model simplifies a Lagrangian stochastic model to create a dispersal kernel that estimates the likelihood a propagule will travel a given distance (Katul et al., 2005). Our dispersal kernel takes the form of the inverse Gaussian distribution

$$p(r) = \left(\frac{\lambda'}{2\pi r^3} \right)^{\frac{1}{2}} \exp \left[-\frac{\lambda'(r - \mu')^2}{2\mu'^2 r} \right] \quad (3)$$

that is a **slight adaptation**³ from equation 5b in Katul et al. (2005), using r to denote dispersal distance. Here, λ' is the location parameter and μ' is the scale parameter, which depend on environmental and plant-specific properties of the study system. (We use λ' for consistency with notation in related papers, but λ' the dispersal location parameter should not be confused with λ the geometric growth rate.) The location and scale parameters are defined as $\lambda' = (H/\sigma)^2$ and $\mu' = HU/F$; these are functions of the height H of seed release, wind speed U at seed release height, seed terminal velocity F , and the turbulent flow parameter σ that depends on both wind speed and local vegetation roughness. We parameterized the WALD dispersal kernel using windspeed data from the SEV-LTER weather station nearest our study site (cite) and seed terminal velocity data from laboratory-based seed-drop experiments. Methods for our seed data collection and technical details of dispersal kernel modeling are provided in Appneix A.

Spatial integral projection model

We used a spatial integral projection model to piece together seed dispersal and density-dependent demography, and generate predictions for the rate of shrub expansion that results from this combination of local and spatial processes. The spatially explicit model builds upon the non-spatial model (Eq. 1) and adds a spatial variable (z, z') such that demographic transitions occur across both time and space according to a combined

³*unclear what this refers to*

380 demography-dispersal kernel \tilde{K} :

$$381 \quad n(x', z', t + 1) = \int_{-\infty}^{+\infty} \int_L^U \tilde{K}(x', x, z', z, \tilde{n}(z, t)) n(x, z, t) dx dz \quad (4)$$

382 Here, $\tilde{K}(x', x, z', z, \tilde{n}(z, t))$ is the rate of transition from size x and location z to size x'
 383 and location z' given density $\tilde{n}(z, t)$ at location z . As before, \tilde{n} is a function of pop-
 384 ulation structure – in our model, weighted local density – but here integrated over an
 385 explicit competitive “neighborhood”: $\tilde{n}(z, t) = \int_{z-h}^{z+h} \int_L^U x n(x, z, t) dx dz$ where h repre-
 386 sents neighborhood size in the units of z .

387 Given that the shrub population at this site is approximately homogeneous perpen-
 388 dicular to the direction of encroachment, expansion is modelled as a wave moving in one
 389 dimension. A spatial integral projection model (SIPM) is used to estimate the speed at
 390 which encroachment occurs; such a model incorporates the effects of variation in traits
 391 like plant size that stage-structured models, such as those described in Neubert and
 392 Caswell (2000), do not capture. According to Jongejans et al. (2011), a general SIPM
 393 can be formulated as

$$394 \quad \mathbf{n}(x_2, z_2, t + 1) = \iint \tilde{K}(x_2, x_1, z_2, z_1) \mathbf{n}(x_1, z_1, t) dx_1 dz_1 \quad (5)$$

395 where x_1 and x_2 are locations of individuals of a particular size before and after one unit of
 396 time, and z_1 and z_2 are the respective sizes. The vector \mathbf{n} indicates the population density
 397 of each size, and \tilde{K} is a kernel that combines dispersal with demography. Though this
 398 SIPM represents a continuous spectrum of shrub sizes and densities, it was implemented
 399 by discretising the above integral with a 200 x 200 matrix, as this makes calculations
 400 significantly more tractable.

401 Movement of the wave is determined by the components of the combined disper-
 402 sal/demography kernel \tilde{K} , which is of the same form as that used in Jonjegans et al.

403 (2011). Here,

$$404 \quad \tilde{K}(x_2, x_1, z_2, z_1) = K(x_2 - x_1)Q(z_2 - z_1) + \delta(x_2 - x_1)G(z_2 - z_1) \quad (6)$$

405 and K is the dispersal kernel, Q a reproduction function, G a growth function, and δ
 406 the Dirac delta function. G is derived from the model for annual growth ratio, and Q is
 407 derived from the reproductive structures model as well as other factors including number
 408 of seeds per reproductive structure, probability of recruitment from seed, and recruit
 409 size. Both G and Q give the probability of transition between sizes; in the case of G , this
 410 is the probability of growing from one specific size to another, and in the case of Q the
 411 probability that an individual of a specific size produces a recruit of a specific size. The
 412 product of K and Q represents the production and dispersal of motile propagules, while
 413 the product of G and δ represents the growth of sessile individuals.

414 Given growth function G and the reproduction function Q , the speed of the moving
 415 wave can be calculated as

$$416 \quad c^* = \min_{s>0} \left[\frac{1}{s} \ln(\rho_s) \right] \quad (7)$$

417 where s is the wave shape parameter and ρ_s is the dominant eigenvalue of the kernel \mathbf{H}_s
 418 (Jongejans et al., 2011). This estimate for the wavespeed is valid under the assumption
 419 that population growth decreases monotonically as conspecific density increases, with the
 420 highest rates of growth occurring at the lowest population densities (Lewis et al., 2006).
 421 The kernel \mathbf{H}_s is defined as

$$422 \quad \mathbf{H}_s = M(s)Q(z_2 - z_1) + G(z_2 - z_1) \quad (8)$$

423 where $M(s)$ is the moment-generating function of the dispersal kernel (Jongejans et al.,
 424 2011). For one-dimensional dispersal, this moment-generating function can be estimated

425 as

$$426 \quad M(s) = \frac{1}{N} \sum_{i=1}^n I_0(sr_i) \quad (9)$$

427 where r is the dispersal distance for each observation, and I_0 is the modified Bessel
428 function of the first kind and zeroth order (Skarpaas and Shea, 2007). In order to obtain
429 M , numerous dispersal distances were simulated from the dispersal kernel $K(r)$ described
430 in the previous section, with over 2000 replications for each shrub height increment of 1
431 cm. This was performed over the range from the lowest possible dispersal height to the
432 maximum shrub height. Once $M(s)$ was obtained for dispersal at each shrub height, \mathbf{H}_s
433 and c^* were calculated for each value of s ; this was done for values of s ranging from 0
434 to 2, as it is this range in which c^* occurs.

435 Estimates of the wavespeed were bootstrapped for a total of 1000 replicates. Each
436 bootstrap replicate recreated size- and density-dependent demographic models using 80%
437 resampling on the original demographic data, and recreated dispersal kernels also using
438 80% resampling on the wind speeds and seed terminal velocities. Between replicates,
439 the structure of the demographic models was kept constant, though coefficient estimates
440 were not; this approach, while effectively ignoring model uncertainty, has the benefit of
441 increasing computational efficiency, which is especially useful given the time-consuming
442 nature of numerically estimating the many dispersal kernels used in the model.

443 Results

444 Encroachment re-surveys

445 Re-surveys along two permanent transects revealed virtually no change the in the creosote
446 expansion wave over 12 years (Fig. 2). There were local changes in percent cover: on
447 average cover increased by XX% between surveys. However, there was no clear indication
448 that the leading edge of the creosote shrubland has advanced (the modest right-ward shift
449 on both transects is within the range of measurement error).

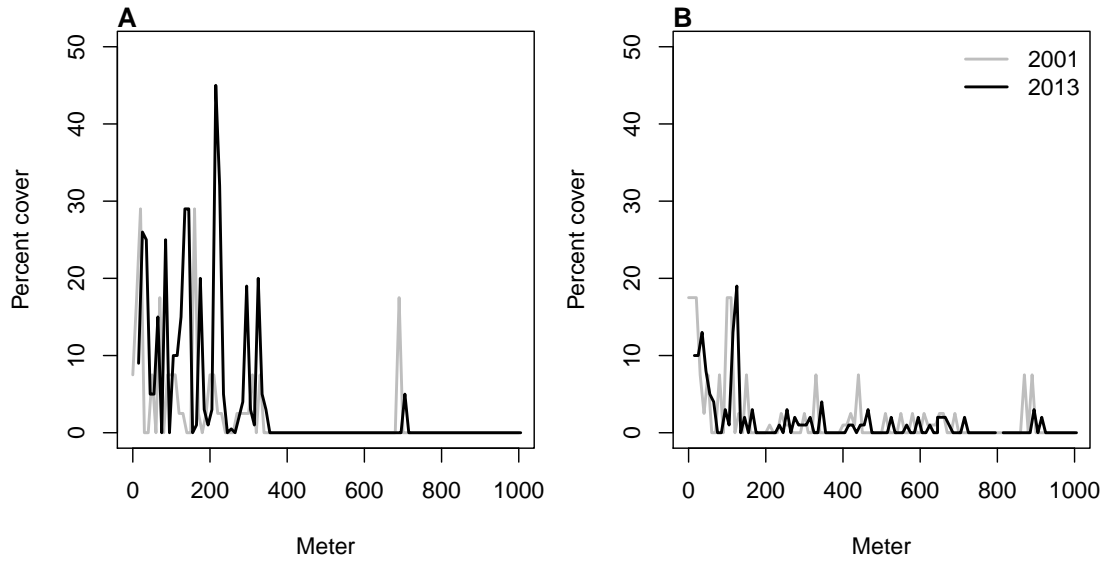


Figure 2: Re-surveys of shrub cover along two permanent trasects (A,B) surveyed in 2001 and 2013.

Size and density dependent demography

Demographic data from naturally occurring and transplanted individuals revealed strong size- and density-dependence in demographic vital rates. For most sizes and vital rates, local density had negative demographic effects. Statistical support for size- and density-dependence is provided in Table XX, which provides AIC rankings for candidate models based on the completed (not bootstrapped) data set.

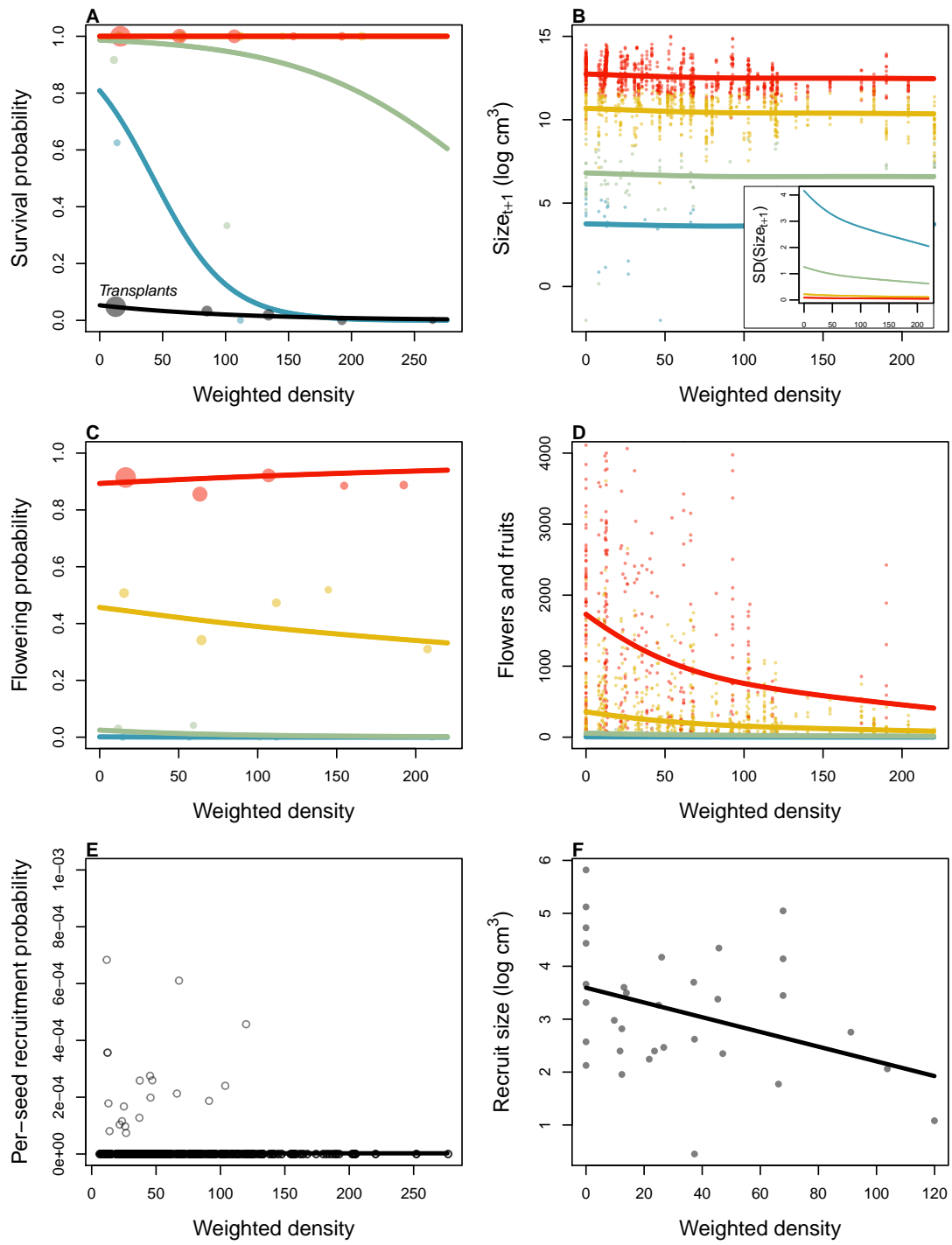


Figure 3: Size- and density-dependence in demographic vital rates.

456 **Survival** Among naturally occurring plants, survival of large, established individuals
457 was very high (Fig. 3A). We observed relatively few mortality events (XX out of XX)
458 and nearly all of these were among new recruits that we detected during the study. The
459 probability of survival at these small sizes declined with increasing density.

460 Survival of transplants was very low, lower even than survival of similarly-sized, nat-
461 urally occurring recruits (Fig. 3B). However, the transplant results support the general
462 pattern of negative density dependence in survival. Among the XX survivors, XX of them
463 occurred in transect windows in the bottom 10th percentile of weighted shrub density.

464 SHORT PARAGRAPH SUMMARIZING SMALLER-SCALE ANALYSIS IN AP-
465 PENDIX.

466 **Growth** Current size was strongly predictive of future size, as expected, and there
467 was weak negative density dependence in mean future size conditioned on current size
468 (Fig. 3C). However, there was a stronger signal of density dependence in the standard
469 deviation of future size (Fig. 3C, inset). Plants at low density exhibited greater variance
470 in growth trajectories and this was especially true at the smallest sizes. Thus, large
471 increases in the size of new recruits were most likely under low-density conditions.

472 **Flowering and fruit production**

473 **Recruitment**

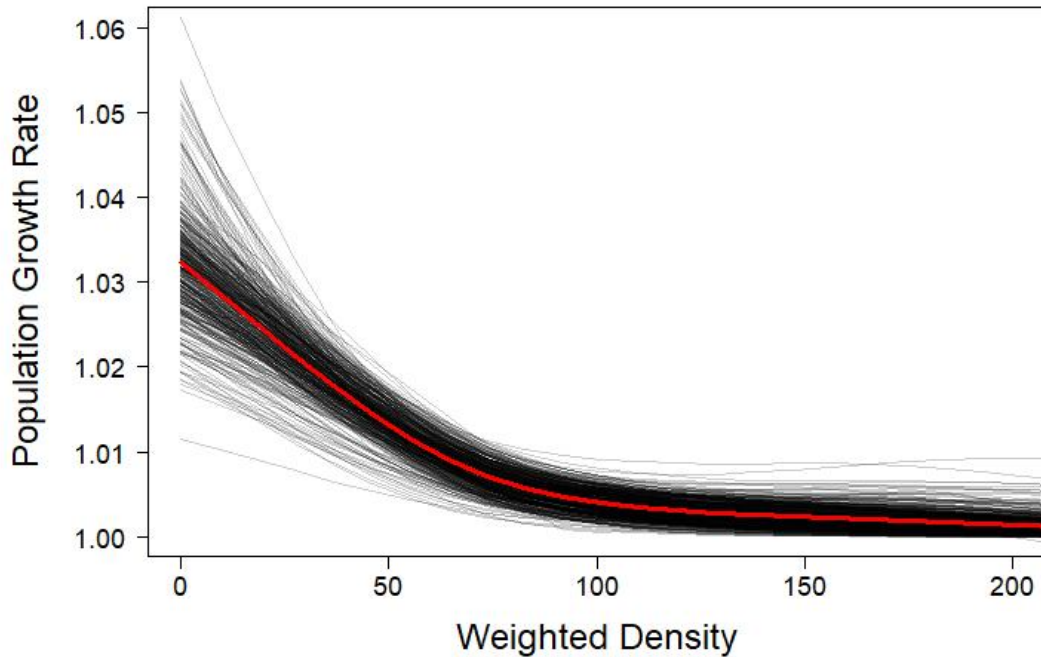


Figure 4: Density dependence in the geographic population growth rate (λ).

474 **Population growth rate** The speed of encroachment at the study site as estimated
 475 by the SIPM is rather slow; as can be seen in Figure 5, the low-density wavefront moves
 476 at approximately 0.5 cm/yr under normal conditions and at 1 cm/yr under the best
 477 seedling survival conditions observed in the dataset. These improved conditions were
 478 observed due to above-average rainfall that occurred after greenhouse-grown seedlings
 479 were transplanted to the site. Population growth in this low-density region of the mov-
 480 ing wave is also low, with a geometric growth rate of $\lambda \approx 1.006$ and even lower rates of
 481 growth the higher-density regions behind; in the higher-survival scenario the maximum
 482 rate increases to $\lambda \approx 1.013$, with growth still decreasing as density increases. For both
 483 scenarios, the decrease in population growth rate with increasing density was monotonic
 484 across the range of observed standardised densities, as is shown in Figure 5. This suggests
 485 that an Allee effect is likely not present in this population, as the highest rate of popula-

tion growth is found at the lowest density vanguard of the encroaching population. Thus, the conditions necessary for equation 9 to be valid are satisfied, and these wavespeeds are applicable for a pulled-wave scenario in which no Allee effects are present.

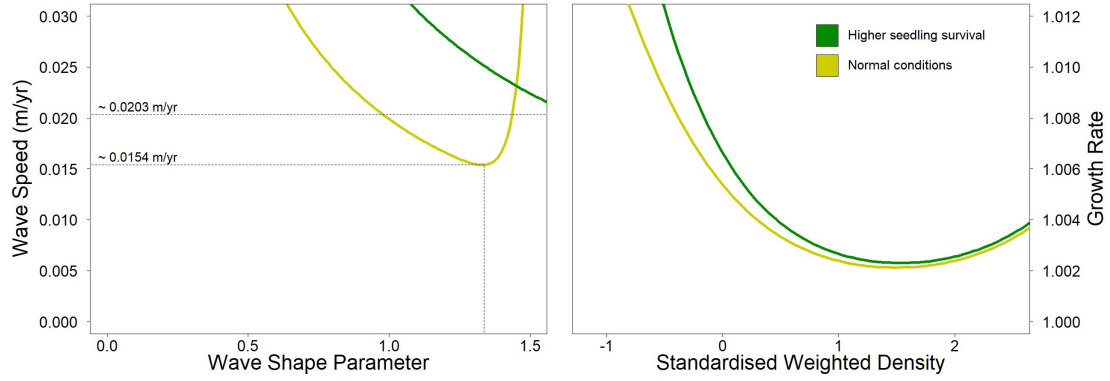


Figure 5: Estimated encroachment wave speeds (left) and geometric rates of population growth (right) for higher post-rainfall seedling survival and normal conditions.

As the speed of encroachment is quite limited, so is the extent of wind dispersal. Long distance dispersal events, while more common for taller shrubs than their shorter counterparts, are still uncommon overall. For the tallest shrub height of 1.98 m, only 0.32% of propagules exceed a dispersal distance of 5 m, and 0.02% exceed 10 m. At 1 m, or approximately half the tallest shrub height, long distance dispersal is even less likely, with 0.0046% of propagules exceeding a dispersal distance of 5 m and 0.0009% exceeding 10 m. Given that the median shrub height is only 0.64 m, the occurrence of long-distance wind dispersal in most of the shrub population is highly improbable, and the few instances in which it occurs will only be limited to the tallest shrubs. Thus, as Figure 6 demonstrates, shorter dispersal distances dominate; even for the tallest shrub, 81% of seeds fall within only a metre of the plant, and this percentage increases as shrub height decreases. Dispersal kernels have their highest probability density at dispersal distances between 2 and 8 cm from the shrub; here, as shrub height increases, the most probable dispersal distance slightly increases while maximum probability density

503 decreases. Regardless of the shrub height, most dispersal will occur very close to the
 504 plant, though increases in shrub height dramatically increase the likelihood of dispersal
 505 at longer distances. It is clear that the shape of the height-dependent dispersal kernel
 506 $K(r)$ varies greatly among the shrub population given the large range of shrub heights
 507 observed; shrubs at lower heights have more slender kernels with most of the seeds dis-
 508 persing closer to the plant, while taller shrubs have kernels with much fatter tails and
 509 are more capable of longer-distance dispersal.

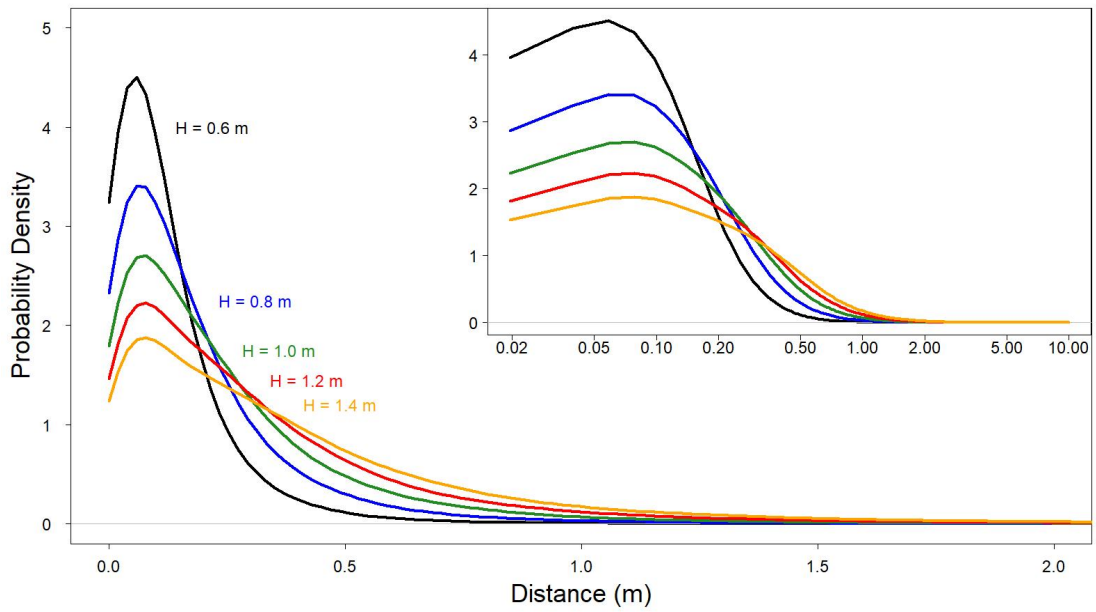


Figure 6: Dispersal kernels, with each colour representing a selected shrub height. The inset plot is the same as the large plot, though with a logarithmic x-axis to more easily show differences in dispersal probability at smaller distances.

510 Density and size dependence are evident in all 4 of the demographic rates, with
 511 coefficients for each model displayed in Table 2. For growth, reproduction, and survival,
 512 density dependence is mostly negative and monotonic; this is not the case for probability
 513 of flowering, where shrub size seems to be more important than the effects of density alone
 514 and suggests that larger shrubs have a higher probability of flowering than their smaller

515 counterparts. This, along with size and density dependence in growth and reproduction,
516 is shown in Figure 7. Size dependence is positive for reproduction, as would be expected
517 since larger plants typically produce more flowers and fruits. However, annual growth
518 decreases as size increases; this could be in part due to the annual growth in this study
519 being quantified as a proportion relative to the shrub's initial size. While larger shrubs
520 may produce more plant material over a year in terms of absolute volume, smaller shrubs
521 produce less but can still have higher annual growth in terms of the percentage of volume
522 added relative to their initial volume. When compared to density, shrub size is a much
523 stronger predictor of survival, with significant differences in mortality rates depending on
524 shrub size. For small shrubs, mortality is exceptionally high, and increases in volume for
525 these shrubs only slightly increase the likelihood of survival. However, after shrubs reach
526 a logarithmic volume of approximately 7.3, they are almost guaranteed to survive, with
527 survival rates near 100% persisting regardless of any further size increases. Interestingly,
528 though most recruits were found at lower densities, the probability of recruitment from
529 seed displays positive density dependence; the probability of recruitment was still very
530 low, though, with a baseline rate of approximately 2 recruits per 10,000 seeds.

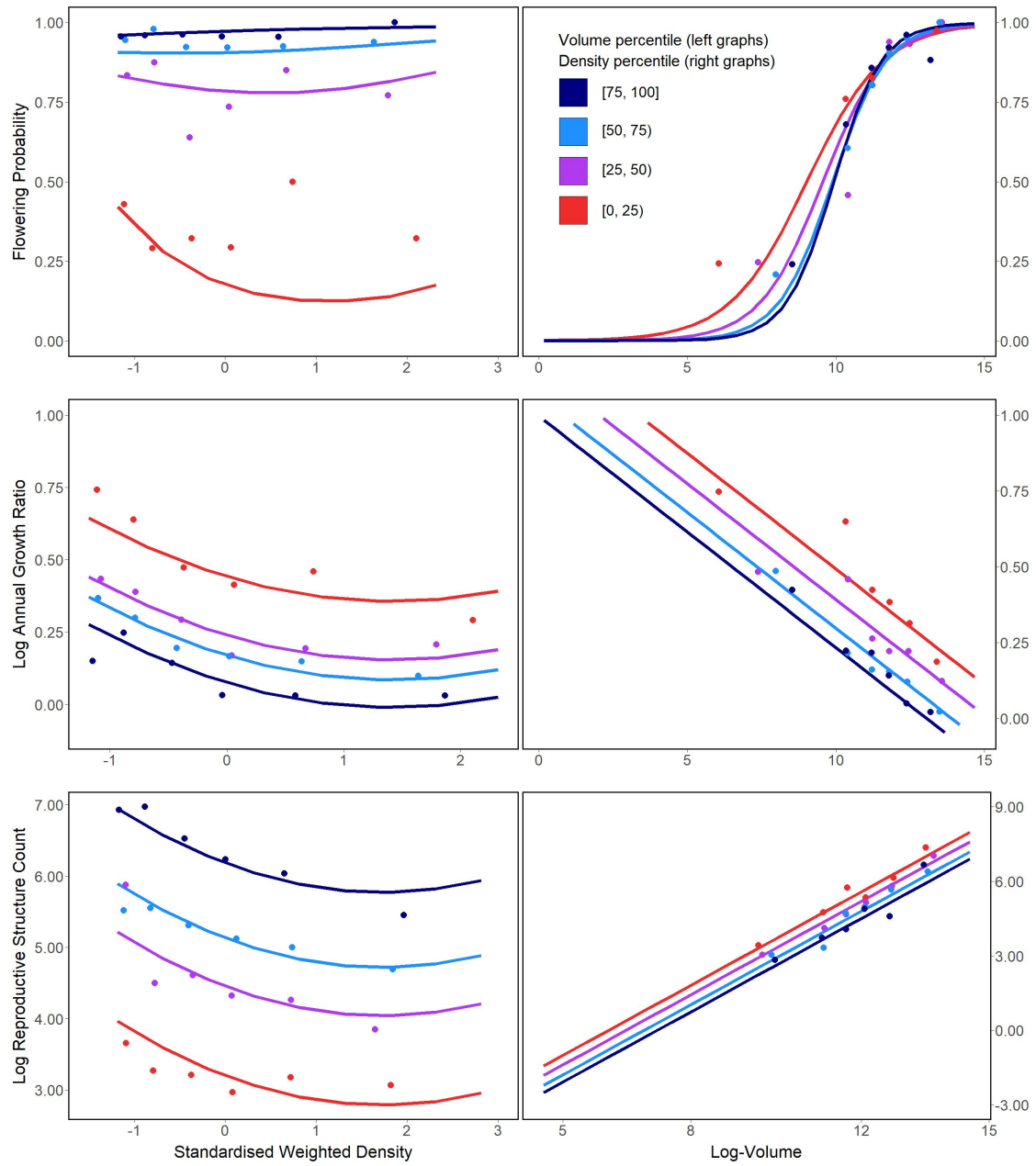


Figure 7: Flowering probability (top row), log annual growth ratio (centre row), and log reproductive structure count (bottom row) at all four sampling sites. In the left column of graphs, the three response variables are shown as a function of density for each of four volume quartiles, with each quartile containing six density bins; in the right column, the opposite occurs, with response variables shown as functions of four volume quartiles that each contain six density bins. Graphs quantifying the number of reproductive structures include data only on plants that flowered.

Discussion

The slow movement of the encroaching creosotebush wave at the Sevilleta LTER site can likely be contributed to a combination of three factors: short dispersal distances with extremely limited long-distance dispersal events, very low probability of recruitment from seed, and high seedling mortality. These three barriers, when combined, form a formidable challenge to the establishment of new shrubs at the low-density front of the wave. First, a seed must travel far enough to avoid competition with the parent shrub, which is unlikely given the dispersal kernels shown in Figure 2. Even if the seed manages to be dispersed this far, its chances of becoming a seedling are low. Caching and consumption by seed-eaters such as a variety of seed-harvesting ants (Whitford, 1978; Whitford et al., 1980; Lei, 1999) and the kangaroo rat *Dipodomys merriami* (Chew and Chew, 1970) decreases the amount of seeds available for germination. However, reduction in germination caused by destruction of seeds may be partly mitigated by the more favourable germination conditions that these seeds can experience when cached underground (Chew and Chew, 1970). Many of the remaining seeds will still fail to germinate, and in the unlikely event that germination does occur, seedlings will likely die given the high rates of mortality observed in smaller shrubs. Such high rates of creosotebush seedling mortality have been observed in other studies as well (Boyd and Brum, 1983; Bowers et al., 2004), probably due to a combination of herbivory, competition, and abiotic stresses.

However, as low as they are, the wavespeed estimates given in this paper are still conservative estimates for reasons mostly related to dispersal. First, it is important to note that the dispersal kernels used here, while they account for variation in factors such as wind speed and terminal velocity, may underestimate the distances that shrub propagules travel. Because the WALD model assumes that terminal velocity is reached immediately upon seed release, seeds in the estimate thus take a shorter time to fall

557 and have less time to be transported by wind, and the true frequency of long-distance
558 dispersal events may thus be greater than what is estimated here. Second, dispersal at the
559 study site could occur through additional mechanisms other than wind. For example,
560 secondary dispersal through runoff from significant rainfall events can transport seeds
561 (Thompson et al., 2014), and given that long-distance dispersal by bird and subsequent
562 species divergence is thought to be responsible for creosotebush being in North America
563 in the first place (Wells and Hunziker, 1976), short-distance dispersal by other animals
564 at the study site likely occurs. As mentioned above, seeds are transported by seed-
565 harvesting ants and granivorous mammals, where they are often stored in caches that
566 can be appreciable distances from the parent shrubs. Whether transportation occurs via
567 ant or rodent, creosotebush seeds can be moved significantly further than wind alone
568 can, though many of these seeds are eventually consumed.

569 Despite the more conservative estimates our model yields, the estimated rate of dis-
570 persal in creosotebush populations at the Sevilleta National Wildlife Refuge is consistent
571 with observations from the past 50-60 years, as creosotebush expansion during this time
572 has been minimal (Moreno-de las Heras et al., 2016). However, it cannot explain the
573 long-term increases in creosotebush cover at the study site, as total encroachment over
574 the past 150 years is much greater than what would be expected given the encroachment
575 rates derived by our models. Such a discrepancy is likely due to much of the expansion
576 occurring in an episodic fashion, with short times during which rapid encroachment oc-
577 curs due to favourable environmental conditions. This could be due in part to seedling
578 recruitment, which is a factor that strongly limits creosotebush expansion, being rare
579 and episodic. For example, Allen et al. (2008) estimate that a major recruitment event
580 occurred at this site in the 1950s, which is supported by photographic evidence from
581 Milne et al. (2003) of a drought-driven expansion during this time. Moreno-de las Heras
582 et al. (2016) estimate that after this expansion, several smaller creosotebush recruitment
583 events occurred in decadal episodes. However, such events can be highly localised and

584 may not necessarily occur at the low-density front of encroachment, which could explain
585 how these recruitment events can still coexist with lack of encroachment in the recent
586 past.

587 Overall, our observations and model highlight three aspects of creosotebush encroach-
588 ment that should be the focus of future studies seeking to obtain better estimates of
589 encroachment rates. First, negative density dependence in survival, growth, and repro-
590 duction is demonstrated, along with size dependence. The clear dependence on size and
591 conspecific density suggests that they both should be considered when estimating cre-
592 osotebush expansion and quantifying the demographic variation that contributes to it.
593 Second, wind dispersal in these shrubs is quite limited; though the dispersal kernels seen
594 here are typical in the sense that they are characterised by high near-plant dispersal and
595 exceptionally low long-distance dispersal, the scale across which such dispersal occurs
596 is small, with most seeds landing within only 1 m of the shrub. Wind dispersal alone
597 may be an underestimate of the true amount of dispersal occurring, and future work
598 should seek to incorporate the effects of dispersal by runoff and animals so that a more
599 representative model of total dispersal can be obtained. Finally, encroachment is slow or
600 even stagnates, but only most of the time. Though our encroachment speed estimates
601 are representative of creosotebush populations for most years, the significant expansion
602 seen over larger time scales suggests that there is episodic expansion in other years; while
603 our model is consistent with the recent stagnation in creosotebush encroachment at the
604 Sevilleta LTER site, a model that also includes interannual variability in factors such
605 as survival and recruitment would be able to better account for instances of episodic
606 population expansion that are characteristic of this location.

607 Acknowledgements

608 Author contributions

609 Data accessibility

610 References

- 611 Allen, A., W. Pockman, C. Restrepo, and B. Milne. 2008. Allometry, growth and
612 population regulation of the desert shrub *Larrea tridentata*. *Functional Ecology* pages
613 197–204.
- 614 Bowers, J. E., R. M. Turner, and T. L. Burgess. 2004. Temporal and spatial patterns in
615 emergence and early survival of perennial plants in the Sonoran Desert. *Plant Ecology*
616 **172**:107–119.
- 617 Boyd, R. S., and G. D. Brum. 1983. Postdispersal reproductive biology of a Mojave Desert
618 population of *Larrea tridentata* (Zygophyllaceae). *American Midland Naturalist* pages
619 25–36.
- 620 Brandt, J. S., M. A. Haynes, T. Kuemmerle, D. M. Waller, and V. C. Radeloff. 2013.
621 Regime shift on the roof of the world: Alpine meadows converting to shrublands in
622 the southern Himalayas. *Biological Conservation* **158**:116–127.
- 623 Buffington, L. C., and C. H. Herbel. 1965. Vegetational changes on a semidesert grassland
624 range from 1858 to 1963. *Ecological monographs* **35**:139–164.
- 625 Bullock, J. M., S. M. White, C. Prudhomme, C. Tansey, R. Perea, and D. A. Hooftman.
626 2012. Modelling spread of British wind-dispersed plants under future wind speeds in
627 a changing climate. *Journal of Ecology* **100**:104–115.

628 Cabral, A., J. De Miguel, A. Rescia, M. Schmitz, and F. Pineda. 2003. Shrub encroach-
629 ment in Argentinean savannas. *Journal of Vegetation Science* **14**:145–152.

630 Chew, R. M., and A. E. Chew. 1970. Energy relationships of the mammals of a desert
631 shrub (*Larrea tridentata*) community. *Ecological Monographs* pages 2–21.

632 Davis, C., 2015. sgt: Skewed Generalized T Distribution Tree. URL [https://CRAN.](https://CRAN.R-project.org/package=sgt)
633 [R-project.org/package=sgt](https://CRAN.R-project.org/package=sgt).

634 D’Odorico, P., J. D. Fuentes, W. T. Pockman, S. L. Collins, Y. He, J. S. Medeiros,
635 S. DeWekker, and M. E. Litvak. 2010. Positive feedback between microclimate and
636 shrub encroachment in the northern Chihuahuan desert. *Ecosphere* **1**:1–11.

637 D’Odorico, P., G. S. Okin, and B. T. Bestelmeyer. 2012. A synthetic review of feedbacks
638 and drivers of shrub encroachment in arid grasslands. *Ecohydrology* **5**:520–530.

639 Gandhi, S. R., E. A. Yurtsev, K. S. Korolev, and J. Gore. 2016. Range expansions
640 transition from pulled to pushed waves as growth becomes more cooperative in an
641 experimental microbial population. *Proceedings of the National Academy of Sciences*
642 **113**:6922–6927.

643 Gardner, J. L. 1951. Vegetation of the creosotebush area of the Rio Grande Valley in
644 New Mexico. *Ecological Monographs* **21**:379–403.

645 Gibbens, R., R. McNeely, K. Havstad, R. Beck, and B. Nolen. 2005. Vegetation changes
646 in the Jornada Basin from 1858 to 1998. *Journal of Arid Environments* **61**:651–668.

647 Goslee, S., K. Havstad, D. Peters, A. Rango, and W. Schlesinger. 2003. High-resolution
648 images reveal rate and pattern of shrub encroachment over six decades in New Mexico,
649 USA. *Journal of Arid Environments* **54**:755–767.

650 Grover, H. D., and H. B. Musick. 1990. Shrubland encroachment in southern New Mexico,

651 USA: an analysis of desertification processes in the American Southwest. *Climatic*
652 *change* **17**:305–330.

653 Hsieh, C.-I., and G. G. Katul. 1997. Dissipation methods, Taylor’s hypothesis, and
654 stability correction functions in the atmospheric surface layer. *Journal of Geophysical*
655 *Research: Atmospheres* **102**:16391–16405.

656 Huang, H., L. D. Anderegg, T. E. Dawson, S. Mote, and P. D’Odorico. 2020. Crit-
657 ical transition to woody plant dominance through microclimate feedbacks in North
658 American coastal ecosystems. *Ecology* **101**:e03107.

659 Jongejans, E., K. Shea, O. Skarpaas, D. Kelly, and S. P. Ellner. 2011. Importance of
660 individual and environmental variation for invasive species spread: a spatial integral
661 projection model. *Ecology* **92**:86–97.

662 Katul, G., A. Porporato, R. Nathan, M. Siqueira, M. Soons, D. Poggi, H. Horn, and
663 S. A. Levin. 2005. Mechanistic analytical models for long-distance seed dispersal by
664 wind. *The American Naturalist* **166**:368–381.

665 Keitt, T. H., M. A. Lewis, and R. D. Holt. 2001. Allee effects, invasion pinning, and
666 species’ borders. *The American Naturalist* **157**:203–216.

667 Kelleway, J. J., K. Cavanaugh, K. Rogers, I. C. Feller, E. Ens, C. Doughty, and N. Sain-
668 tilan. 2017. Review of the ecosystem service implications of mangrove encroachment
669 into salt marshes. *Global Change Biology* **23**:3967–3983.

670 Knapp, A. K., J. M. Briggs, S. L. Collins, S. R. Archer, M. S. BRET-HARTE, B. E.
671 Ewers, D. P. Peters, D. R. Young, G. R. Shaver, E. Pendall, et al. 2008. Shrub
672 encroachment in North American grasslands: shifts in growth form dominance rapidly
673 alters control of ecosystem carbon inputs. *Global Change Biology* **14**:615–623.

- 674 Kot, M., M. A. Lewis, and P. van den Driessche. 1996. Dispersal data and the spread of
675 invading organisms. *Ecology* **77**:2027–2042.
- 676 Lei, S. A. 1999. Ecological impacts of *Pogonomyrmex* on woody vegetation of a *Larrea*-
677 *Ambrosia* shrubland. *The Great Basin Naturalist* pages 281–284.
- 678 Lewis, M., and P. Kareiva. 1993. Allee dynamics and the spread of invading organisms.
679 *Theoretical Population Biology* **43**:141–158.
- 680 Lewis, M. A., M. G. Neubert, H. Caswell, J. S. Clark, and K. Shea, 2006. A guide
681 to calculating discrete-time invasion rates from data. Pages 169–192 *in* *Conceptual*
682 *ecology and invasion biology: reciprocal approaches to nature*. Springer.
- 683 Mabry, T. J., J. H. Hunziker, D. Difeo Jr, et al. 1978. Creosote bush: biology and
684 chemistry of *Larrea* in New World deserts. Dowden, Hutchinson & Ross, Inc.
- 685 Maddox, J. C., and S. Carlquist. 1985. Wind dispersal in Californian desert plants:
686 experimental studies and conceptual considerations. *Aliso: A Journal of Systematic*
687 *and Evolutionary Botany* **11**:77–96.
- 688 Milne, B. T., D. I. Moore, J. L. Betancourt, J. A. Parks, T. W. Swetnam, R. R. Par-
689 menter, and W. T. Pockman. 2003. Multidecadal drought cycles in south-central New
690 Mexico: Patterns and consequences. Oxford University Press: New York, NY.
- 691 Moreno-de Las Heras, M., R. Díaz-Sierra, L. Turnbull, and J. Wainwright. 2015. Assess-
692 ing vegetation structure and ANPP dynamics in a grassland–shrubland Chihuahuan
693 ecotone using NDVI–rainfall relationships. *Biogeosciences* **12**:2907–2925.
- 694 Moreno-de las Heras, M., L. Turnbull, and J. Wainwright. 2016. Seed-bank structure
695 and plant-recruitment conditions regulate the dynamics of a grassland-shrubland Chi-
696 huahuan ecotone. *Ecology* **97**:2303–2318.

- 697 Mugasi, S., E. Sabiiti, and B. Tayebwa. 2000. The economic implications of bush
698 encroachment on livestock farming in rangelands of Uganda. *African Journal of Range*
699 *and Forage Science* **17**:64–69.
- 700 Nathan, R., G. G. Katul, G. Bohrer, A. Kupařinen, M. B. Soons, S. E. Thompson,
701 A. Trakhtenbrot, and H. S. Horn. 2011. Mechanistic models of seed dispersal by wind.
702 *Theoretical Ecology* **4**:113–132.
- 703 Neubert, M. G., and H. Caswell. 2000. Demography and dispersal: calculation and
704 sensitivity analysis of invasion speed for structured populations. *Ecology* **81**:1613–
705 1628.
- 706 Oba, G., E. Post, P. Syvertsen, and N. Stenseth. 2000. Bush cover and range condition
707 assessments in relation to landscape and grazing in southern Ethiopia. *Landscape*
708 *ecology* **15**:535–546.
- 709 Pan, S., and G. Lin. 2012. Invasion traveling wave solutions of a competitive system
710 with dispersal. *Boundary Value Problems* **2012**:120.
- 711 Parizek, B., C. M. Rostagno, and R. Sottini. 2002. Soil erosion as affected by shrub
712 encroachment in northeastern Patagonia. *Rangeland Ecology & Management/Journal*
713 *of Range Management Archives* **55**:43–48.
- 714 Peters, D. P., and J. Yao. 2012. Long-term experimental loss of foundation species:
715 consequences for dynamics at ecotones across heterogeneous landscapes. *Ecosphere*
716 **3**:1–23.
- 717 Ratajczak, Z., J. B. Nippert, and S. L. Collins. 2012. Woody encroachment decreases
718 diversity across North American grasslands and savannas. *Ecology* **93**:697–703.
- 719 Raupach, M. 1994. Simplified expressions for vegetation roughness length and zero-

720 plane displacement as functions of canopy height and area index. *Boundary-Layer*
721 *Meteorology* **71**:211–216.

722 Ravi, S., P. D’Odorico, S. L. Collins, and T. E. Huxman. 2009. Can biological invasions
723 induce desertification? *The New Phytologist* **181**:512–515.

724 Reed, M., L. Stringer, A. Dougill, J. Perkins, J. Athopheng, K. Mulale, and N. Favretto.
725 2015. Reorienting land degradation towards sustainable land management: Linking
726 sustainable livelihoods with ecosystem services in rangeland systems. *Journal of envi-*
727 *ronmental management* **151**:472–485.

728 Reynolds, J. F., R. A. Virginia, P. R. Kemp, A. G. De Soyza, and D. C. Tremmel. 1999.
729 Impact of drought on desert shrubs: effects of seasonality and degree of resource island
730 development. *Ecological Monographs* **69**:69–106.

731 Roques, K., T. O’connor, and A. R. Watkinson. 2001. Dynamics of shrub encroach-
732 ment in an African savanna: relative influences of fire, herbivory, rainfall and density
733 dependence. *Journal of Applied Ecology* **38**:268–280.

734 Schlesinger, W. H., and A. M. Pilmanis. 1998. Plant-soil interactions in deserts. *Biogeo-*
735 *chemistry* **42**:169–187.

736 Schlesinger, W. H., J. A. Raikes, A. E. Hartley, and A. F. Cross. 1996. On the spatial
737 pattern of soil nutrients in desert ecosystems: ecological archives E077-002. *Ecology*
738 **77**:364–374.

739 Schlesinger, W. H., J. F. Reynolds, G. L. Cunningham, L. F. Huenneke, W. M. Jarrell,
740 R. A. Virginia, and W. G. Whitford. 1990. Biological feedbacks in global desertification.
741 *Science* **247**:1043–1048.

742 Sirami, C., and A. Monadjem. 2012. Changes in bird communities in Swaziland savannas

743 between 1998 and 2008 owing to shrub encroachment. *Diversity and Distributions*
744 **18**:390–400.

745 Skarpaas, O., and K. Shea. 2007. Dispersal patterns, dispersal mechanisms, and invasion
746 wave speeds for invasive thistles. *The American Naturalist* **170**:421–430.

747 Sullivan, L. L., B. Li, T. E. Miller, M. G. Neubert, and A. K. Shaw. 2017. Density depen-
748 dence in demography and dispersal generates fluctuating invasion speeds. *Proceedings*
749 *of the National Academy of Sciences* **114**:5053–5058.

750 Taylor, C. M., and A. Hastings. 2005. Allee effects in biological invasions. *Ecology*
751 *Letters* **8**:895–908.

752 Thompson, S. E., S. Assouline, L. Chen, A. Trahktenbrot, T. Svoray, and G. G. Katul.
753 2014. Secondary dispersal driven by overland flow in drylands: Review and mechanistic
754 model development. *Movement ecology* **2**:7.

755 Trollope, W., F. Hobson, J. Danckwerts, and J. Van Niekerk. 1989. Encroachment and
756 control of undesirable plants. *Veld management in the Eastern Cape* pages 73–89.

757 Turnbull, L., J. Wainwright, and R. E. Brazier. 2010. Changes in hydrology and erosion
758 over a transition from grassland to shrubland. *Hydrological Processes: An Interna-*
759 *tional Journal* **24**:393–414.

760 Van Auken, O. 2009. Causes and consequences of woody plant encroachment into western
761 North American grasslands. *Journal of environmental management* **90**:2931–2942.

762 Van Auken, O. W. 2000. Shrub invasions of North American semiarid grasslands. *Annual*
763 *review of ecology and systematics* **31**:197–215.

764 Vasek, F. C. 1980. Creosote bush: Long-lived clones in the Mojave Desert. *American*
765 *Journal of Botany* **67**:246–255.

- 766 Veit, R. R., and M. A. Lewis. 1996. Dispersal, population growth, and the Allee ef-
767 fect: dynamics of the house finch invasion of eastern North America. *The American*
768 *Naturalist* **148**:255–274.
- 769 Wang, M.-H., M. Kot, and M. G. Neubert. 2002. Integrodifference equations, Allee
770 effects, and invasions. *Journal of mathematical biology* **44**:150–168.
- 771 Wells, P. V., and J. H. Hunziker. 1976. Origin of the creosote bush (*Larrea*) deserts of
772 southwestern North America. *Annals of the Missouri Botanical Garden* pages 843–861.
- 773 Whitford, W., E. Depree, and P. Johnson. 1980. Foraging ecology of two chihuahuan
774 desert ant species: *Novomessor cockerelli* and *Novomessor albigenu*. *Insectes Sociaux*
775 **27**:148–156.
- 776 Whitford, W. G. 1978. Structure and seasonal activity of Chihuahua desert ant commu-
777 nities. *Insectes Sociaux* **25**:79–88.
- 778 Wiernga, J. 1993. Representative roughness parameters for homogeneous terrain.
779 *Boundary-Layer Meteorology* **63**:323–363.
- 780 Williams, J. L., T. E. Miller, and S. P. Ellner. 2012. Avoiding unintentional eviction
781 from integral projection models. *Ecology* **93**:2008–2014.
- 782 Wood, S. 2017. *Generalized Additive Models: An Introduction with R*. 2 edition.
783 Chapman and Hall/CRC.

Appendix A

In order to create the dispersal kernel, we first take the wind speeds at measurement height z_m and correct them to find wind speed U for any height H by using the logarithmic wind profile ⁴

$$U = \frac{1}{H} \int_{d+z_0}^H \frac{u^*}{K} \log \left(\frac{z-d}{z_0} \right) dz \quad (10)$$

given in Bullock et al. (2012) equation 6, with the notation slightly modified. Here, z is the height above the ground, K is the von Karman constant, and u^* is the friction velocity. The zero-plane displacement d and roughness length z_0 are surface roughness parameters that, for a grass canopy height h above the ground, are approximated by $d \approx 0.7h$ and $z_0 \approx 0.1h$. These estimates are from Raupach (1994) for a canopy area index $\Lambda = 1$ in which the sum of grass canopy elements is equal to the unit area being measured. A 0.15 m grass height at our study site gives $d = 0.105$ and z_0 , which are suitable approximations for grassland (Wiernga, 1993). Calculations of u^* were done using equation A2 from Skarpaas and Shea (2007), in which

$$u^* = KU_m \left[\log \left(\frac{z_m - d}{z_0} \right) \right]^{-1} \quad (11)$$

and U_m is the mean wind velocity at the measurement height z_m . Values for the turbulent flow parameter σ were then calculated using the estimate made by Skarpaas and Shea (2007) in their equation A4, where

$$\sigma = 2A_w^2 \sqrt{\frac{K(z-d)u^*}{C_0U}} \quad (12)$$

and C_0 is the Kolmogorov constant. A_w is a constant that relates vertical turbulence to friction velocity and is approximately equal to 1.3 under the assumptions of above-

⁴ *We need to describe and cite the wind data used here.*

canopy flow made by Skarpaas and Shea (2007), based off calculations from Hsieh and Katul (1997). In addition, the assumption that $z = H$ was made in order to make the calculation of σ more feasible.⁵

The values from the previous three equations give us the necessary information to calculate μ' and λ' , thus allowing us to create the WALD distribution $p(r)$. However, the base WALD model does not take into account variation in wind speeds or seed terminal velocities, which limits its applicability in systems where such variation is present. In order to account for this variation, we integrate the WALD model over distributions of these two variables using the same method as Skarpaas and Shea (2007). Additionally, the WALD model assumes seed release from a single point source, which is not realistic for creosote bush; because seeds are released across the entire height of the shrub rather than from a point source, we integrated $p(r)$ across the uniform distribution from the grass canopy height to the shrub height. Thus, under the assumptions that the height at which a seed is located does not affect its probability of being released and that seeds are evenly distributed throughout the shrub, this gives the dispersal kernel $K(r)$, where

$$K(r) = \iiint p(F)p(U)p(z)p(r) dF dU dz \quad (13)$$

and $p(F)$ and $p(U)$ are the PDFs of the terminal velocity F and wind speed U , respectively, and $p(z)$ is the uniform distribution from h to H .

Dispersal data collection The distribution $p(F)$ in the integral above was constructed using experimentally determined seed terminal velocities. This was done by using laboratory-based seed release experiments with a high-speed camera and motion tracking software to determine position as a function of time. We then used the Levenberg-Marquardt algorithm to solve a quadratic-drag equation of motion for F . Before seeds were released, they were dried, dyed with yellow fluorescent powder, and then

⁵ *Can you describe this assumption in biological terms?*

829 put against a black background to improve visibility and make tracking easier. While the
830 powder added mass to the seeds, this added mass only yielded an approximately 2.5%
831 increase, likely having little effect on terminal velocities. Measurements were conducted
832 for 48 seeds that were randomly chosen from a seed pool derived from different plants,
833 and then an empirical PDF of terminal velocities was constructed using the data. Con-
834 structing $p(U)$ involved creating an empirical PDF of hourly wind speeds using data from
835 a Sevilleta LTER meteorological station (Five Points), the station closest to our transects.
836 We used wind speed data collected from 1988 to 2010.⁶

⁶ *Most SEV data sets have a doi, so ideally we should cite the wind speed data.*